An Enhanced Preamble of PRACH Frame for Low-Altitude Long-Distance Integrated Sensing and Communication System

Xiaoyang Wang †, Xiao Yu, Zhengchun Xu, Xiaoyou Yu *,†, Zhaohan Zhang, Qian Ma, Zengjie Shao

Posted Date: 3 March 2026

doi: 10.20944/preprints202603.0126.v1

Keywords: PRACH; OCC-ZC sequences; preamble; ISAC; low-altitude

 doi:10.20944/preprints202603.0126.v1

Article

An Enhanced Preamble of PRACH Frame for Low-Altitude Long-Distance Integrated Sensing and Communication System

Xiaoyang Wang [1,2,3,†], Xiao Yu [1,2,3], Zhengchun Xu [1,2,3], Xiaoyou Yu [4,*,†], Zhaohan Zhang [4], Qian Ma [4] and Zengjie Shao [4]

[1] CRSC Low-Altitude Intelligence Technology Co., Ltd
[2] National Railway Administration Innovation Base of Low-altitude applications and safety (Engineering Research Center)
[3] Beijing Key Laboratory of Intelligent Management and Control of Low-altitude Airspace
[4] College of Computer Science and Electronic Engineering, Hunan University
* Correspondence: yuxiaoyou@hnu.edu.cn
† The corresponding author and the first author contribute equally to this work.

Abstract

In this paper, we propose an enhanced preamble scheme for the physical random access channel (PRACH) applied to low-altitude integrated sensing and communication (ISAC) systems, aiming to expand the sensing capability of traditional mobile networks with PRACH frames based on ZC sequences. To enable the network to possess target sensing capability before successful terminal access, we transform PRACH from a mere initial access channel into an ISAC system capable of supporting high-speed terminal access and user equipment sensing by introducing a time-frequency orthogonal block structure and orthogonal cover codes (OCCs). Specifically, we first derive the Cramér-Rao lower bound (CRLB) for estimating the distance and velocity of user equipment using OCC-ZC sequences, and establish the evaluation metric for communications named detection probabilities. Then, the ISAC problem is formulated as a multi-objective optimization function. Since the multi-objective optimization problem is non-convex, we propose the NSAG-II algorithm to solve it, simultaneously improving the estimation accuracy of distance and velocity in the sensing aspect and the detection probability in the communication aspect.

Keywords: PRACH; OCC-ZC sequences; preamble; ISAC; low-altitude

1. Introduction

With the emergence and development of low-altitude traffic and transportation, a large number of aircraft equipped with sensing and communication devices are being widely used [1–3]. However, the surge in the number of radio-frequency devices in low-altitude wireless networks poses severe challenges to the existing PRACH-based random access in low-altitude long-distance communication scenarios. M. Hua et al. [4] have theoretically analyzed that in PRACH, traditional ZC sequences are extremely sensitive to frequency offsets. Their work demonstrates that in a Doppler shift environment, the ideal autocorrelation properties of ZC sequences are seriously disrupted, leading to timing ambiguities and errors in timing estimation, which directly affect the reliability of random access [5]. However, the increase in the number of RF devices exacerbates the shortage of spectrum resources. Integrated Sensing and Communication (ISAC) technology, which shares spectrum and hardware resources, is a key approach to improving resource utilization [6]. In 4G systems (LTE), the signals and protocol stack were designed around communication functions, and the system inherently lacked integrated sensing and communication capabilities. In the development stage of the 5G system, the initial versions did not consider ISAC as a core function, and the sensing capabilities remained in the preliminary exploration phase [7]. It was not until 5G-Advanced (5G-A, also known as 5.5G) that ISAC

 doi:10.20944/preprints202603.0126.v1

was formally established as a clear evolution direction and written into vision documents, aiming to deeply integrate sensing functions into communication systems [8]. In current 5G-A research and applications, sensing functions mainly rely on dedicated sensing signals configured after the terminal completes random access or establishes business channels [9]. This "access first, sense later" [10,11] working mode means that the system's sensing capability cannot be activated during the random access phase, creating an "initial sensing blind zone"—that is, the network can only effectively sense the terminal and its surrounding environment after the terminal successfully accesses the network via the Physical Random Access Channel (PRACH) [12,13].

The initial sensing blind zone poses multiple challenges for low-altitude long-distance communication. First, it causes a lag in the detection: since the network cannot obtain any state information about the terminal before access, there is an inevitable time window between the terminal's appearance and its effective detection by the network [14,15]. Second, it creates regulatory loopholes: traditional sensing mechanisms rely on authorized terminals, allowing unauthorized or intentionally evasive rogue aircraft to hide their presence before access [16–18]. Finally, it leads to resource inefficiency: PRACH, as a mandatory signal for every terminal waiting to access the network, carries valuable channel information that fails to be converted into environmental sensing data after access detection is completed, wasting scarce wireless resources [19]. Consequently, it will be a key breakthrough to achieve ISAC.

Previous studies have investigated the design of PRACH in terms of sensing capabilities. Linsalata et al. proposed an OTFS-superimposed PRACH scheme, which enhances delay and Doppler resolution through the superimposition of the OTFS structure, but it requires significant modifications to existing protocols and terminals, increases signal processing complexity, and its performance still deteriorates in strong interference environments [20]. Kumari et al. explored a non-uniform preamble layout virtual waveform design, which, although improving Doppler estimation accuracy by optimizing time-domain intervals, is essentially a trade-off between communication and sensing and does not achieve true functional integration [21]. Accordingly, we found that although there has been research on PRACH sensing, the ultimate sensing performance has not significantly improved. Moreover, to our knowledge, the integrated functionality of sensing and communication in PRACH has rarely been studied. In this paper, we propose a novel, innovative PRACH frame structure design for low-altitude long-distance communication scenarios, aiming to introduce sensing capabilities into PRACH, enabling the network to possess target sensing capability from the very beginning of access.

Before presenting the main contributions of this work, it is necessary to provide a brief overview of the optimization algorithms employed. The system, operating in a low-altitude long-distance Integrated Sensing and Communication (ISAC) scenario, faces multiple constraints and trade-offs among communication reliability, sensing accuracy, and resource efficiency. Traditional single-objective optimization methods are inadequate for simultaneously satisfying these conflicting performance requirements. Therefore, a multi-objective optimization framework is essential to explore reasonable trade-off solutions within the complex system parameter space. This paper adopts the Non-dominated Sorting Genetic Algorithm II (NSGA-II) [22] to jointly optimize parameters such as the Orthogonal Cover Code (OCC) design in the PRACH preamble, transmission power, and bandwidth. The goal is to concurrently enhance the random access success probability, reduce the estimation errors for both range and velocity in sensing, and control resource overhead. The necessity for multi-objective optimization stems from the fact that no single configuration exists in a practical system that can simultaneously optimize communication, sensing, and resource efficiency to their respective extrema. Instead, a set of Pareto-optimal solutions emerges [23], each corresponding to a distinct communication-sensing trade-off strategy. Through the efficient search and sorting mechanisms of the NSGA-II algorithm, the system can obtain a series of feasible configurations under the constraints of power, bandwidth, and codebook. This capability enables the network to flexibly select operational strategies such as "communication-priority", "sensing-priority", or "balanced mode" based on real-time demands, thereby

 doi:10.20944/preprints202603.0126.v1

achieving sustainable and synergistic optimization of ISAC functionalities in resource-constrained environments.

The contributions of this paper are summarized as follows:

1. This paper proposes a novel PRACH framework structure design method based on time-frequency orthogonal block sequences. By introducing the time-frequency orthogonal block structure and orthogonal covering codes (OCCs), the Doppler effect is no longer simply regarded as an interference that needs to be avoided, but is actively utilized as a valuable sensing resource. This changes the physical layer frame structure and signal processing mode of PRACH.

2. In the time domain, the basic ZC sequence repeats N times, thereby forming multiple discrete time blocks. We apply a fixed orthogonal covering code to each time block, thereby adding a new encoding dimension to the traditional sequence dimension. The design of the OCC-ZC sequence is transformed into a weighted optimization problem through detection probability and Cramér-Rao lower bound (CRLB) for communication and target sensing performance, in order to achieve the ISAC function.

3. For the non-convex problem of a multi-objective optimization function, we used the NSGA-II algorithm to solve the optimization problem of OCC-ZC design under resource allocation conditions.

4. We conducted a large number of simulation experiments, and the results showed that the proposed method enables PRACH to achieve the ISAC function, while also ensuring the performance of communication access.

It should be noted that the proposed OCC-ZC preamble introduces additional PRACH resource consumption due to the repetition of the base ZC sequence. This overhead is mainly reflected in the increased preamble duration proportional to the repetition factor M.However, the proposed design is primarily targeted at low-altitude long-distance access scenarios, where the number of simultaneously contending UEs is relatively limited, while access reliability and sensing capability are of higher priority. In such scenarios, PRACH transmission is sporadic rather than continuous, and the additional resource consumption does not significantly affect the whole system capacity. When the system load increases, smaller values of M can be adopted to reduce resource consumption, while larger values of M are preferred in sensing-priority or coverage-limited scenarios. Therefore, the proposed scheme is not intended as a universal replacement for conventional PRACH, but as a flexible enhancement for specific ISAC-oriented scenarios.

The subsequent content of this paper will elaborate on the detailed design and performance of the enhanced PRACH preamble. Chapter 2 systematically describes the frame structure design of the proposed OCC-ZC preamble, including the construction methods of ZC and OCC sequences, and derives the ISAC signal processing flow based on this preamble. It establishes performance analysis models from both sensing and communication perspectives, including the Cramér-Rao lower bound (CRLB) for range and velocity estimation and the closed-form expression for preamble detection probability. Chapter 3 formalizes the preamble design into a multi-objective optimization problem under constraints of transmission power, bandwidth, and orthogonal codebook, aiming to balance the random access success probability, sensing estimation error, and resource consumption cost. To solve this non-convex mixed-integer programming problem, Chapter 4 introduces the NSGA-II algorithm, detailing its steps to obtain a Pareto-optimal solution set via multi-objective evolutionary search. Chapter 5 validates the effectiveness of the proposed scheme in low-altitude long-distance scenarios through extensive simulations, including multi-objective trade-off analysis, comparison of communication detection probability, and assessment of sensing parameter (range and velocity) estimation accuracy. Results show that the OCC-ZC structure improves detection probability while significantly enhancing sensing accuracy. Finally, Chapter 6, summarizes the work and suggests directions for future research.

 doi:10.20944/preprints202603.0126.v1

2. Materials and Methods

2.1. The Random Access Procedure

Motivated by the four-step random access mechanism of the 3GPP standards, Figure 1 illustrates the proposed ISAC random access procedure, which comprises four distinct steps:

Step 1 (Preamble Transmission): The User Equipment (UE) transmits a random access preamble to indicate an access request and assist the Base Station(BS) in achieving uplink initial synchronization. Step 2 (Random Access Response): The BS responds with a Timing Advance (TA) command and a temporary uplink resource grant. Step 3 (Scheduled Transmission): The UE utilizes the allocated resources to transmit specific signaling containing its unique identifier. Step 4 (Contention Resolution): Finally, the BS transmits a contention resolution message to arbitrate access conflicts and establish the final connection.

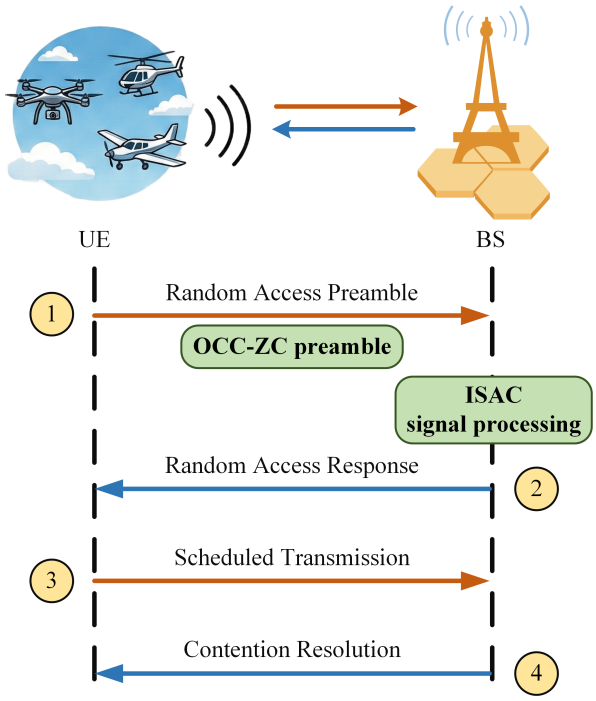

Figure 1. The random access procedure.

The proposed scheme fully preserves the original protocol timing and signaling order, aiming to extend system functionality without disrupting the existing network architecture. In Step 1, the conventional access preamble is replaced by the OCC-ZC preamble designed in this paper. This preamble constructs a specific sequence structure by superimposing OCC onto time-domain repeated sequence blocks. The ISAC signal processing module shown in the figure1 is specifically designed to handle this unique signal format. By leveraging the orthogonality introduced by the OCC, the module processes the received signal to extract Doppler information embedded in the signal phase difference, thereby directly resolving the target's radial velocity, while simultaneously completing standard user access detection. Furthermore, a closed-loop ISAC optimization mechanism is introduced. This module evaluates the communication access success rate and the detection error in real-time and dynamically adjusts the resource allocation parameters. This ensures access performance while maximizing sensing accuracy, achieving a deep integration of communication and sensing in terms of both functionality and resources.

This improved scheme establishes the foundation of the physical layer for the proposed ISAC system. Based on this, the remainder of this paper will elaborate on the specific frame structure design and mathematical model of the OCC-ZC preamble. It will also provide an in-depth analysis of the ISAC signal processing workflow, with a focus on deriving the theoretical performance of communication detection and sensing parameter estimation based on this signal format.

 doi:10.20944/preprints202603.0126.v1

2.2. The Enhanced Preamble of PRACH Frame

2.2.1. The ZC Sequences

As shown in Figure 2 (a), a conventional PRACH preamble consists of a Cyclic Prefix (CP), a base sequence (ZC sequence or short sequence), and a Guard Period (GP). Its length and structure are determined by the preamble format to accommodate different coverage ranges and deployment scenarios. The ZC sequence [24] is adopted to maintain its excellent auto-correlation and cross-correlation properties, providing a foundation for initial timing synchronization. Its discrete-time expression is:

$$z[n] = \exp\left(-j\frac{\pi u n(n+1)}{N_{ZC}}\right), \quad n = 0, 1, \ldots, N_{ZC} - 1 \tag{1}$$

where u is the root index that is coprime with N_{ZC}.

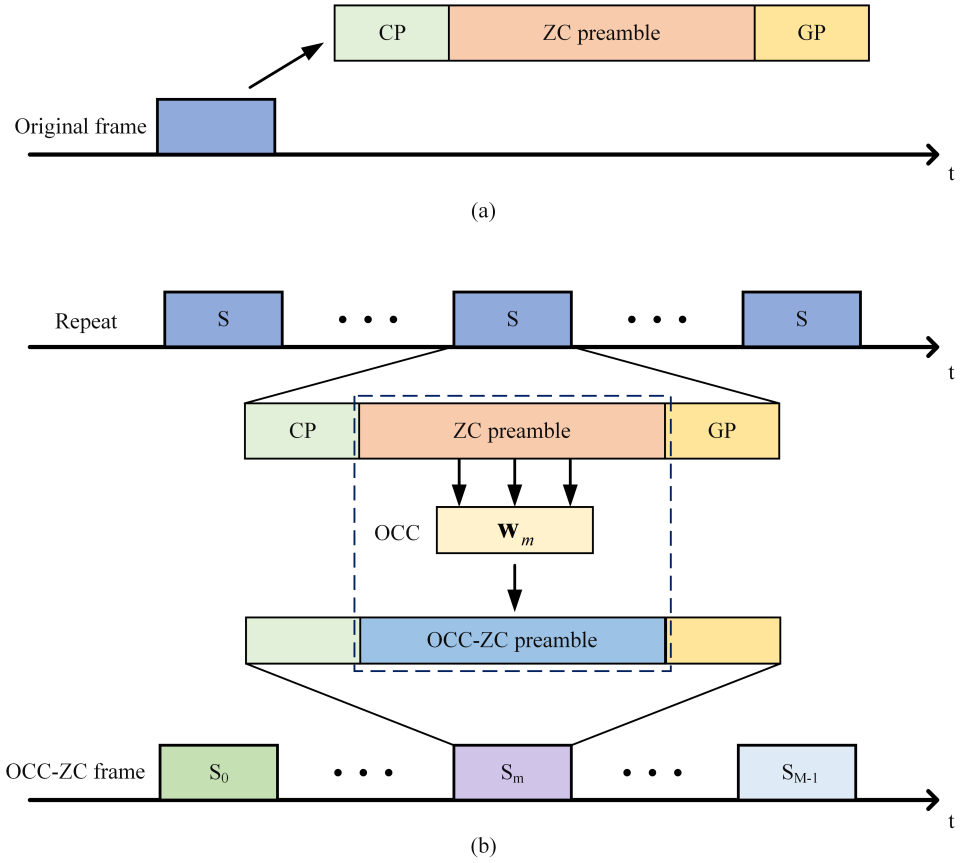

Figure 2. (a) The conventional PRACH frame structure. (b) The OCC-ZC frame structure.

2.2.2. The OCC Sequences

The OCC sequence is a vector made up of M orthogonal kernel function values, whose most fundamental property is orthogonality between sequences. This orthogonality is typically defined through the inner product. Assuming there are two sequences of the OCC code $\mathbf{w}_p$ and $\mathbf{q}_j$, they can be expressed as [25]:

$$\begin{aligned} \mathbf{w}_p &= \left[w_p(0), w_p(1), \ldots, w_p(M-1)\right] \\ \mathbf{w}_q &= \left[w_q(0), w_q(1), \ldots, w_q(M-1)\right] \end{aligned} \tag{2}$$

The inner product between them is defined as

$$\left\langle \mathbf{w}_p, \mathbf{w}_q \right\rangle = \sum_{m=0}^{M-1} w_p(M) \cdot w_q^*(M) \tag{3}$$

 doi:10.20944/preprints202603.0126.v1

where $w_q^*(M)$ denotes the complex conjugate of $w_q(M)$. For real-valued OCC codes (the most common case), the conjugate can be omitted. The orthogonality condition is given by:

$$\langle \mathbf{w}_p, \mathbf{w}_q \rangle = \begin{cases} E, & \text{if } p = q \\ 0, & \text{if } p \neq q \end{cases} \tag{4}$$

where E is a constant that typically represents the energy of the sequence. When $E = 1$, the set of sequences is said to be orthonormal.

2.2.3. The OCC-ZC Preamble

As shown in Figure 2 (b), to simultaneously extract the range and velocity information of user equipment (UE) during the access process, a discernible time-domain structure must be introduced into the signal. This scheme constructs multiple time blocks by repeating the base sequence in the time domain and applies OCC to form a new preamble signal:

$$s[n] = \sum_{m=0}^{M-1} z\left[(n - mL)_{N_{ZC}}\right] \cdot w[m] \cdot \Pi[n - mL], \quad n = 0, 1, \ldots, N_{ZC} - 1 \tag{5}$$

where L is the length of each time block, $\Pi[n]$ is the rectangular window function, and $(\cdot)_{N_{ZC}}$ represents the modulo operation N_{ZC}.

2.3. ISAC Based on the Enhanced Preamble

2.3.1. Sensing

To consider the relative motion between the Low-UE and the base station, the received signal can be modeled as

$$y_r[n] = h_r \cdot s[n - \tau] e^{j2\pi f_d n T_s} + \omega[n] \tag{6}$$

where h_r is the complex reflection coefficient in which the path loss, target cross-section are included, τ is the propagation delay corresponding to the range $R = c\tau/2$, f_d is the Doppler frequency shift corresponding to the velocity $v = \lambda f_d/2$, T_s is the sampling interval, and $\omega[n]$ is the additive white Gaussian noise, $\omega[n] \sim \mathcal{CN}(0, \sigma_r^2)$.

To simultaneously accomplish communication access and sensing, the receiver processing flow requires a block-based correlation process. Perform correlation operations on each time block to obtain the initial channel response of each block. We obtain the following:

$$Y_m(\tilde{\tau}) = \sum_{n-mL}^{(m+1)L-1} y_r[n] \cdot z^*[n - \tilde{\tau} - mL], \quad m = 0, 1, \ldots, M - 1 \tag{7}$$

The receiver does not know which user k transmitted the signal, nor the exact delay τ. Therefore, it is necessary to search over all possible τ and k.

It is known that $Y_m(\bar{\tau})$ contains the modulation information of $w_k[m]$ (if the signal was transmitted by user k).To detect user k, we can multiply $Y_m(\bar{\tau})$ by the candidate OCC code $w_k^*[m]$ and sum over the blocks:

$$S_k(\bar{\tau}) = \sum_{m=0}^{M-1} Y_m(\bar{\tau}) \cdot w_k^*[m] \tag{8}$$

Assuming the transmitting user is k_0 and $\bar{\tau} = \tau$, and letting $P_z = \sum_{k=0}^{L-1} |z[k]|^2$ denote the sequence energy, then $Y_m(\tau) \approx h_r w_{k_0}[m] P_z$. Substituting this, we obtain the following:

$$S_k(\tau) \approx h_r P_z \sum_{m=0}^{M-1} w_{k_0}[m] w_k^*[m], \tag{9}$$

Substituting (3) and (4) into (9), we can obtain

 doi:10.20944/preprints202603.0126.v1

$$S_k(\tau) \approx \begin{cases} h_r P_z M, & k = k_0 \\ 0, & k \neq k_0 \end{cases} \tag{10}$$

To avoid being affected by the phase of h_r, we take the squared magnitude $|S_k(\bar{\tau})|^2$. This value reaches its maximum when $k = k_0$ and $\bar{\tau} = \tau$. Therefore, the detection criterion is:

$$(\hat{k}, \hat{\tau}) = \arg\max_{k,\bar{\tau}} \left| \sum_{m=0}^{M-1} Y_m(\bar{\tau}) \cdot w_k^*[m] \right|^2 \tag{11}$$

This step enables user identification and access.

After finding the correct user $\hat{k}$ and delay $\hat{\tau}$ through (11), we perform a "purification" step:

$$\tilde{Y}_m = Y_m(\hat{\tau}) \cdot W_{\hat{k}}^*[m] \tag{12}$$

where $W_{\hat{k}}[m] \cdot W_{\hat{k}}^*[m] = 1$ for the correct user, the user-specific coding is removed, and the signal energy is coherently combined. For incorrect users, due to the orthogonality of the codes, the results cancel each other out.

After (12), under ideal conditions where channel coherence is maintained across the M blocks, the orthogonality of OCC ensures that interference from other users is suppressed and noise is reduced through coherent combining. Consequently, the dominant component of the purified signal $\tilde{Y}_m$ can be simplified as:

$$\tilde{Y}_m \approx C \cdot e^{j2\pi f_d m T_b} \tag{13}$$

where C is a complex constant, and $T_b = L \cdot T_s$ is the duration of one time block. The phase of the purified signal $\tilde{Y}_m$ increases linearly with the time block index m, and the rate of increase is proportional to the Doppler frequency shift f_d.

In (13), the phase difference eliminates the constant phase offset, retaining only the phase changes caused by motion. In moderate mobility scenarios where channel variation over the preamble duration is dominated by a constant Doppler shift rather than severe fast fading, the model in (13) serves as a valid approximation. Under this approximation, the phase difference method can be applied for velocity estimation, while the delay method is used for range estimation.

1). f_d estimation: According to (13) we can estimate f_d by utilizing the phase difference between adjacent time blocks. From the previous step, we obtain: phase of $\tilde{Y}_m = 2\pi \cdot f_d \cdot T_b \cdot m$. Thus, the phase difference $\Delta\phi$ between signals in two adjacent time blocks is:

$$\Delta\phi = [2\pi \cdot f_d \cdot T_b \cdot (m+1)] - [2\pi \cdot f_d \cdot T_b \cdot m] = 2\pi \cdot f_d \cdot T_b \tag{14}$$

This result means that the phase difference between two adjacent $\tilde{Y}_m$ is a constant value, and this value directly contains the Doppler frequency shift f_d we are seeking.

Mathematically, the most efficient way to calculate the phase difference between two complex numbers Z_1 and Z_2 is to compute $Z_2 \cdot (Z_1^*)$ and then take the phase angle ($\angle$) of this product. Therefore, for our signal, we have:

$$\Delta\phi = \angle[\tilde{Y}_{m+1} \cdot \tilde{Y}_m^*] \tag{15}$$

Substituting the conclusion from (15) into (14), we can obtain

$$\angle[\tilde{Y}_{m+1} \cdot \tilde{Y}_m^*] = 2\pi \cdot f_d \cdot T_b \tag{16}$$

Then, for any pair of adjacent blocks, we can estimate $f_d = \frac{1}{2\pi T_b} \cdot \angle[\tilde{Y}_{m+1} \cdot \tilde{Y}_m^*]$. To obtain a more accurate and robust estimate, we perform the same calculation for all $M-1$ pairs of adjacent blocks and take the average, and the Doppler frequency shift is accurately estimated.

 doi:10.20944/preprints202603.0126.v1

$$\hat{f}_d = \frac{1}{2\pi T b(M-1)} \sum_{m=0}^{M-2} \angle\left(Y_{m+1}(\hat{\tau}) w^*[m+1] \cdot (Y_m(\hat{\tau}) w^*[m])^*\right) \tag{17}$$

where $T_b = LT_s$ is the block duration. The radial velocity is then given by:

$$\hat{v} = \frac{\lambda \hat{f}_d}{2} \tag{18}$$

The detected timing delay is used to estimate the UE's range, which is given by:

$$\hat{R} = \frac{c \cdot \hat{\tau}}{2} \tag{19}$$

To avoid ambiguity, the phase difference must satisfy $|\Delta\phi| < \pi$.This imposes a constraint on the maximum detectable Doppler shift: $f_{d,max} < \frac{1}{2T_b}$. Consequently, the maximum unambiguous radial velocity is:

$$v_{max} = \frac{\lambda}{4T_b} \tag{20}$$

2.3.2. CRLB for Parameter Estimation in Sensing

Parameter estimation is very important for sensing, and its accuracy is usually measured by the CRLB, which is the lower bound for any unbiased estimator. In the setting considered in this paper, we focus on estimating the parameter vector of $\boldsymbol{\theta} = [\tau, f_d]^T$. According to (13), we find that our estimator essentially estimates the frequency of a complex sinusoidal signal. To obtain the CRLB for estimating $\boldsymbol{\theta}$, we first define the phase observations as:

$$\phi_m = j2\pi f_d m T_b + v_m, \quad v_m \sim \mathcal{CN}\left(0, \sigma_\phi^2\right) \tag{21}$$

At high SNR, the phase noise variance $\sigma_\phi^2 \approx \frac{1}{2\mathrm{SNR}_b}$, where $\mathrm{SNR}_b = |C|^2/\sigma^2$ is the block SNR.

According to (21), observation vector $\phi = [\phi_0, \phi_1, \ldots, \phi_{M-1}]^T$ is subject to the probability density function (PDF):

$$p(\phi; f_d) = \frac{1}{\left(2\pi\sigma_\phi^2\right)^{M/2}} \exp\left[-\frac{1}{2\sigma_\phi^2} \sum_{m=0}^{M-1} (\phi_m - 2\pi f_d m T_b)^2\right] z \tag{22}$$

According to the PDF in (43), the likelihood function can be formulated as

$$\ln p(\phi; f_d) = -\frac{M}{2} \ln\left(2\pi\sigma_\phi^2\right) - \frac{1}{2\sigma_\phi^2} \sum_{m=0}^{M-1} (\phi_m - 2\pi f_d m T_b)^2 \tag{23}$$

For the OCC-ZC signal, due to the excellent ambiguity function properties of ZC sequences, the coupling between delay and Doppler is minimal, and the Fisher information matrix is approximately diagonal:

$$\boldsymbol{I}(\boldsymbol{\theta}) \approx \begin{bmatrix} I_{\tau\tau} & 0 \\ 0 & I_{f_d f_d} \end{bmatrix} = - \begin{bmatrix} E\left[\frac{\partial^2 \ln p}{\partial \tau^2}\right] & 0 \\ 0 & E\left[\frac{\partial^2 \ln p}{\partial f_d^2}\right] \end{bmatrix} \tag{24}$$

Plugging (23) into (28), the elements in the FIM matrix are derived

$$I_{f_d f_d} = -E\left[\frac{\partial^2 \ln p}{\partial f_d^2}\right] = \frac{(2\pi T_b)^2}{\sigma_\phi^2} \sum_{m=0}^{M-1} m^2 \tag{25}$$

 doi:10.20944/preprints202603.0126.v1

Using the formula $\sum_{m=0}^{M-1} m^2 = \frac{(M-1)M(2M-1)}{6}$, we can obtain:

$$I_{f_d f_d} = \frac{(2\pi T_b)^2}{\sigma_\phi^2} \cdot \frac{(M-1)M(2M-1)}{6} \tag{26}$$

By substituting $\sigma_\phi^2 \approx 1/(2\mathrm{SNR}_b)$ into (26), we can obtain

$$\mathrm{Var}\left(\hat{f}_d\right) \geq \frac{1}{I_{f_d f_d}} = \frac{3}{2\pi^2 T_b^2 \mathrm{SNR}_b \cdot M(M-1)(2M-1)} \tag{27}$$

Then, the CRLB matrix on $\boldsymbol{\theta}$ is the inverse of $\boldsymbol{I}(\boldsymbol{\theta})$, given by

$$\begin{bmatrix} \mathrm{CRLB}(\tau) & 0 \\ 0 & \mathrm{CRLB}(f_d) \end{bmatrix} = \begin{bmatrix} I_{\tau\tau} & 0 \\ 0 & I_{f_d f_d} \end{bmatrix}^{-1} \tag{28}$$

According to $v = \frac{\lambda f_d}{2} = \frac{c f_d}{2 f_c}$, we can obtain $\mathrm{CRLB}(v)$ by using the scale properties of CRLB, given by

$$\mathrm{CRLB}(v) = \left(\frac{\lambda}{2}\right)^2 \cdot \mathrm{CRLB}(f_d) = \frac{3\lambda^2}{8\pi^2 T_b^2 \mathrm{SNR}_b \cdot M(M-1)(2M-1)} \tag{29}$$

Similarly, we can obtain the $\mathrm{CRLB}(\tau)$.

$$I_{\tau\tau} = 8\pi^2 \mathrm{SNR} \cdot \beta^2 \tag{30}$$

where SNR is the total SNR, $\beta^2 = \frac{\int_{-B/2}^{B/2} f^2 |Z(f)|^2 df}{\int_{-B/2}^{B/2} |Z(f)|^2 df}$ is the mean-square bandwidth, $Z(f)$ represents the magnitude spectrum of the continuous-time Fourier transform of the ZC sequence.

From $R = c\tau/2$, we can obtain

$$\mathrm{CRLB}(R) = \left(\frac{c}{2}\right)^2 \cdot \mathrm{CRLB}(\tau) = \frac{c^2}{32\pi^2 \mathrm{SNR}_{\text{total}} \cdot \beta^2} \tag{31}$$

The Root Mean Square Error (RMSE) is a practical metric for evaluating the estimation accuracy, defined as:

$$\mathrm{RMSE}(\hat{\theta}) = \sqrt{E[(\hat{\theta} - \theta)^2]} \tag{32}$$

where $\hat{\theta}$ denotes the estimator of parameter θ (e.g., range R or velocity v). $E(\cdot)$ denotes the mathematical expectation. For an unbiased estimator, the RMSE is related to the variance $\mathrm{Var}(\hat{\theta})$ by:

$$\mathrm{RMSE}(\hat{\theta}) = \sqrt{\mathrm{Var}(\hat{\theta})} \tag{33}$$

The Cramér–Rao Lower Bound (CRLB) provides a theoretical lower bound on the variance of any unbiased estimator:

$$\mathrm{Var}(\hat{\theta}) \geq \mathrm{CRLB}(\theta) \tag{34}$$

Therefore, for an efficient estimator (which achieves the CRLB), the RMSE approaches the square root of the CRLB at high signal-to-noise ratio (SNR):

$$\mathrm{RMSE}(\hat{\theta}) \approx \sqrt{\mathrm{CRLB}(\theta)} \tag{35}$$

2.3.3. Communication

According to [26], the success of the Random Access Channel (RACH) process depends mainly on the successful transmission of the PRACH preamble, and the probability of correct detection of the PRACH preamble is an important communication metric. Motivated by this, we study the detection

 doi:10.20944/preprints202603.0126.v1

probability of OCC-ZC sequences in order to measure the communication performance of PRACH in a quantitative manner.

The $v[n]$ represents the additive Gaussian noise at the receiver side with zero mean and covariance $N0, \quad v[n] \sim \mathcal{CN}(0, \sigma_c^2)$. The received signal can be expressed by

$$y_c[n] = h_c s[n] + v[n], \tag{36}$$

where h_c is the coefficient of the communication channel, assumed constant on the M blocks. The correlation output for the m-th block can be expressed by:

$$X_m = \sum_{k=0}^{N_{ZC}-1} y_c[mN_{ZC} + k] \cdot z^*[k] = h_c w[m] N_{ZC} + V_m, \tag{37}$$

where $\quad V_m \sim \mathcal{CN}(0, E_z \sigma_c^2)$.

We assume that perfect channel estimation and coherent combining, the detector multiplies each X_m by the conjugate of the estimated channel and OCC code:

$$Y = \sum_{m=0}^{M-1} w^*[m] X_m = h_c M N_{ZC} + \sum_{m=0}^{M-1} w^*[m] V_m, \tag{38}$$

We select the real part of the combined output Y as the final detection statistic T. Under hypothesis H_0 ($h_c = 0$), T is contributed only by noise, which can be given by:

$$T \sim \mathcal{N}\left(0, \frac{M N_{ZC} \sigma_c^2}{2}\right), \tag{39}$$

Under hypothesis H_1, the T follows a Gaussian distribution with mean $|h_c| M N_{ZC}$ and variance $\frac{M N_{ZC} \sigma_c^2}{2}$, then:

$$T \sim \mathcal{N}\left(|h_c| M N_{ZC}, \frac{M N_{ZC} \sigma_c^2}{2}\right), \tag{40}$$

Let the detection threshold be η . The false alarm probability is $P_{fa} = \Pr(\Re(Y) > \eta \mid H_0)$, and the detection probability is $P_d = \Pr(\Re(Y) > \eta \mid H_1)$. Accordingly, the detection probability can be represented as

$$P_d = Q\left(Q^{-1}\left(P_{fa}\right) - \sqrt{\frac{2 M N_{ZC} |h_c|^2}{\sigma_c^2}}\right), \tag{41}$$

where $Q(x) = \frac{1}{\sqrt{2\pi}} \int_x^\infty e^{-t^2/2} dt$ is the Q-function and $Q^{-1}(x)$ is the inverse Q-function.

2.3.4. ISAC

Figure 3 shows the framework of the enhanced PRACH preamble based ISAC systems, in which present the close-loop signal processing flow of ISAC based on the OCC-ZC preamble. This framework is designed to seamlessly integrate user equipment access and sensing capabilities within a single transmission while dynamically optimizing resource configuration through a feedback mechanism. In the phase of receiving PRACH frames from the UE, the BS first detect and separate OCC-ZC sequences $y[n]$ preamble from PRACH frames, then initiates the Block-based Correlation Process, and progress to the OCC user separation phase. During this phase, the system leverages the orthogonality of OCC codes to perform coherent combining and interference cancellation. This ensures precise isolation of the target user signal from surrounding noise and interference.

 doi:10.20944/preprints202603.0126.v1

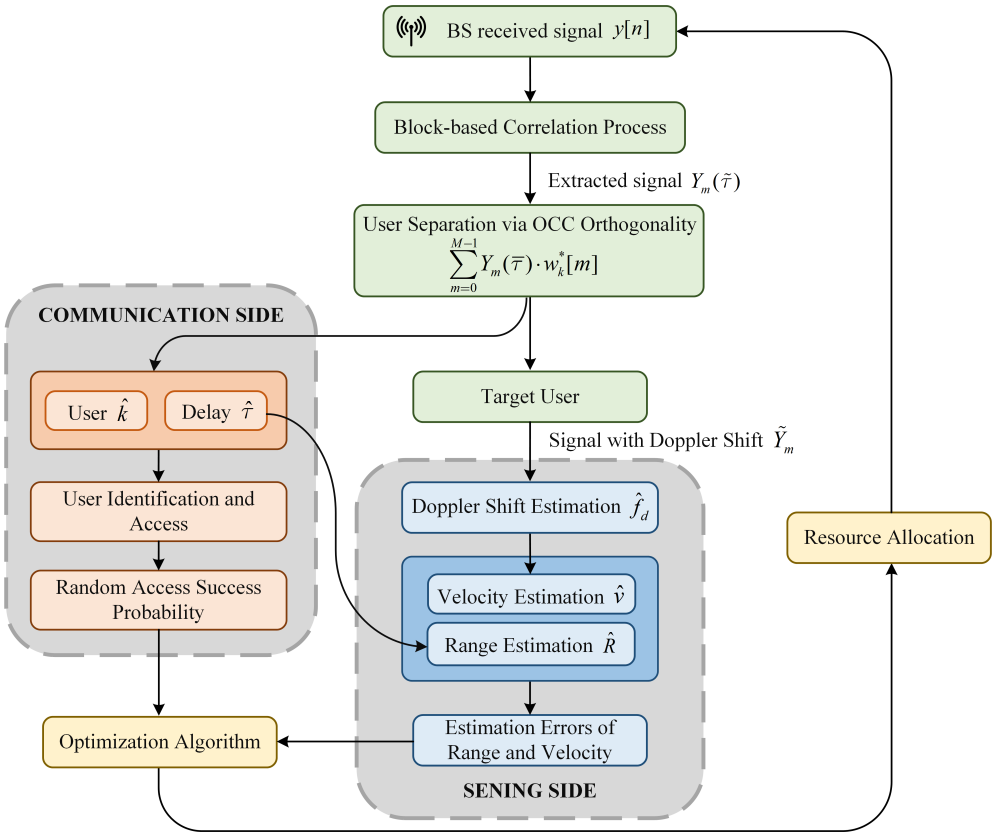

Figure 3. The framework of enhanced PRACH preamble based ISAC systems.

The signal processing flow then diverges into two concurrent functional paths. On the communication side, the system conducts user identification and access detection to determine the target user index $\hat{k}$ and initial delay estimate $\hat{\tau}$. It also computes the random access success probability to assess communication link reliability. Simultaneously, on the sensing side, which closely aligns with the communication function, the delay estimate $\hat{\tau}$ assists in estimating Range ($\hat{R}$), while Doppler Shift Estimation is performed independently to derive Velocity ($\hat{v}$). Additionally, estimation errors are calculated using the CRLB theory to evaluate sensing precision.

This tight integration of sensing and preamble detection capabilities inherently ties system performance to resource allocation strategies. Achieving high-precision sensing and reliable access in scenarios involving low-altitude, long-distance communication often requires increased transmission power and additional physical resources. However, unregulated expansion of these parameters can lead to heightened interference with neighboring cells and strain limited time-frequency resources. To address this trade-off, the Optimization Algorithm illustrated at the bottom left corner of Figure 3 is incorporated into the system's closed-loop design. By utilizing real-time feedback, such as access success probabilities and sensing errors, this module resolves optimal configurations under constraints including power, bandwidth, and interference levels. It then directs the Resource Allocation module to adapt the transmission strategy dynamically, for instance, by adjusting repetition count M or transmission power. This approach enables a balanced optimization of communication reliability and sensing accuracy even in dynamic channel conditions. The detailed design of the optimization algorithm will be covered in the subsequent chapters.

3. Problem Formulation

The main objective of this work is to identify an OCC code so that the proposed OCC-ZC preamble signal can be used for PRACH communication and target sensing under transmission-power and orthogonal-codebook constraints.

 doi:10.20944/preprints202603.0126.v1

$\tilde{C}_{\text{resource}}$ represents a resource allocation penalty term, which can adjust weights and resource allocation strategies based on real-time performance feedback. By introducing $\tilde{C}_{\text{resource}}$, power P, and bandwidth resources B can be dynamically allocated between communication and sensing to prevent one function from consuming too many resources and causing a sharp decline in the performance of the other function, which can be written as follows:

$$\tilde{C}_{\text{resource}} = \gamma \cdot \left(\frac{P}{P_{\max}}\right)^2 + \delta \cdot \left(\frac{B}{B_{\max}}\right)^2 \tag{42}$$

Where B is the bandwidth, $\gamma, \delta, \mu \geq 0$ are weighting coefficients that control the cost of resource consumption.

To solve the optimization problem, which involves the joint optimization of the discrete orthogonal codeword w and continuous transmission parameters (power P, bandwidth B, and sensing slot duration T_s), a three-objective optimization framework is adopted. The problem aims to simultaneously balance three competing performance metrics: the random access success probability η_{comm}, the sensing estimation error $\tilde{\epsilon}_{\text{sensing}}$, and the resource consumption cost $\hat{C}_{\text{resource}}$. Its mathematical description is as follows:

$$\begin{aligned} \min \quad & \mathbf{F}(\mathbf{x}) = \left[-\eta_{\text{comm}}(\mathbf{x}),\ \tilde{\epsilon}_{\text{sensing}}(\mathbf{x}),\ \hat{C}_{\text{resource}}(\mathbf{x}) \right]^{\mathrm{T}} \\ \text{s.t.} \quad & \mathbf{w} \in \mathcal{W}_{\text{orthogonal}} \\ & P \leq P_{\max}, \quad B \leq B_{\max} \\ & \eta_{\text{comm}}(\mathbf{x}) \geq \eta_{\min}, \quad \tilde{\epsilon}_{\text{sensing}}(\mathbf{x}) \leq \tilde{\epsilon}_{\max} \end{aligned} \tag{43}$$

where $\mathbf{x} = (w, P, B)$ denotes the vector of decision variables, and $\mathbf{F}(\mathbf{x})$ is the vector of objective functions to be minimized. where $\eta_{\text{comm}}(\mathbf{x})$ is random access success probability, $\tilde{\epsilon}_{\text{sensing}}(\mathbf{x})$ is the normalized estimation errors of range and velocity defined as

$$\tilde{\epsilon}_{\text{sensing}} = \alpha \cdot \frac{\text{CRLB}(R)}{R_{\max^2}} + \beta \cdot \frac{\text{CRLB}(v)}{v_{\max^2}} \tag{44}$$

where $\alpha > 0$ and $\beta > 0$ are dual variables. $R_{\max}$ is the maximum sensing distance required by the system. $v_{\max}$ is the maximum velocity that the system is required to sense.

Problem (43) describes that the OCC-ZC preamble of the PRACH frame realizes ISAC under the constraints of transmission power and the orthogonal codebook.

The continuous variable transmit power P and the orthogonal codeword of the discrete variable $\mathbf{w} \in \mathcal{W}_{\text{orthogonal}}$ form the basic framework of a mixed-integer programming problem. Any optimization problem involving integer variables has a feasible region consisting of a discrete set of points, and discrete sets are non-convex. Consequently, the problem automatically becomes an NP-hard combinatorial optimization problem. Given the non-convex nature of the problem, genetic algorithms can be employed to find locally optimal solutions.

4. The Proposed Algorithm

The optimization problem formulated in Section 3 is inherently a three-objective optimization. Due to the inherent trade-offs among communication performance, sensing accuracy, and resource efficiency, there exists no single global solution that can simultaneously optimize all three objectives to their respective extremes. Instead, a set of Pareto-optimal solutions emerges, where each solution represents the best attainable balance among the three objectives under the given constraints.

To systematically explore this complex high-dimensional trade-off frontier, this paper employs the Non-dominated Sorting Genetic Algorithm II (NSGA-II) [22], a dedicated multi-objective optimization algorithm. NSGA-II can directly handle the aforementioned three-objective optimization problem without requiring a predefined fixed weighting scheme. It effectively searches for and returns a well-distributed set of Pareto-optimal solutions. This solution set provides a decision-making basis for the

 doi:10.20944/preprints202603.0126.v1

network to flexibly select operational strategies, such as "communication-priority", "sensing-priority", or "balanced-mode", according to diverse real-time requirements.

The specific steps of the algorithm are as follows:

1. **Population initialization**
   Within the feasible region satisfying the constraints, randomly generate the initial population P_0, with a total of I individuals. Each individual contains three optimization objective function values: η_{comm}, $\tilde{\epsilon}_{\text{sensing}}$, and $\hat{C}_{\text{resource}}$.
2. **Genetic operations**
   Perform selection, crossover, and mutation operations on the parent population to generate the offspring population. Selection adopts a binary tournament strategy, prioritizing individuals with a lower non-dominated rank or a larger crowding distance for retention. Crossover uses simulated binary crossover to generate new solutions, with a crossover factor p_c controlling the crossover probability. Mutation employs polynomial mutation to enhance local search capability, with a mutation factor p_m controlling the mutation probability, ultimately yielding the offspring population.
3. **Population combination**
   The parent and offspring populations are combined to form a new population.
4. **Non-dominated sorting**
   The merged new population is then divided into hierarchical levels using the non-dominated sorting method. Non-dominated sorting refers to the process of stratifying and ranking all individuals in the population based on Pareto dominance relationships, dividing them into several non-dominated layers. Its essence lies in establishing hierarchical priorities through dominance relationships, thereby providing a foundation for subsequent crowding distance calculations and individual selection.
5. **Crowding distance calculation**
   Next, calculate the crowding distance D_i for individual i in the current population, considering all three objective functions η_{comm}, $\tilde{\epsilon}_{\text{sensing}}$, and $\hat{C}_{\text{resource}}$, as shown below:

$$D_i = \sum_{j=1}^{3} \frac{|y_{i-1,j} - y_{i+1,j}|}{y_j^{\max} - y_j^{\min}} \tag{45}$$

   where $y_{i-1,j}$ and $y_{i+1,j}$ represent the j-th optimization objective function values of the two individuals adjacent to individual i after sorting, and $y_j^{\max}$ and $y_j^{\min}$ denote the maximum and minimum values of the j-th optimization objective in the current population. The crowding distance reflects the crowding degree among individuals; a larger crowding distance indicates sparser distribution of individuals, leading to better diversity of the solution set.
6. **Selection of individuals**
   First, individuals at lower non-dominated ranks are prioritized for retention. When selection is required among individuals within the same rank, those with larger crowding distances are given priority. This process continues until the number of individuals reaches I, thereby generating a new parent population.
7. **Iteration**
   Repeat steps 2 to 6 until the maximum number of evolutionary iterations is reached, obtaining the Pareto approximate optimal solution set.

The process of population sorting and selection is shown in Figure 4.

 doi:10.20944/preprints202603.0126.v1

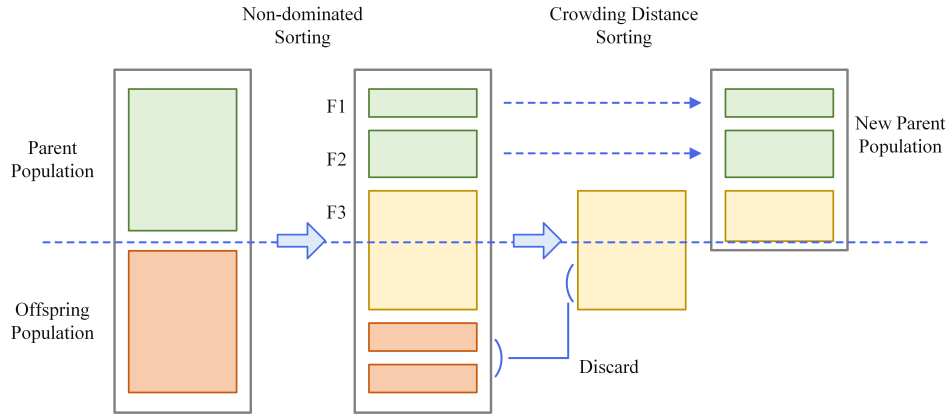

Figure 4. The process of population sorting and selection.

Specifically, the algorithm aims to enhance the random access success rate and uplink throughput on the communication side, optimize Doppler velocity estimation accuracy and target detection probability on the sensing side, while minimizing resource consumption cost $\hat{C}_{\text{resource}}$. Leveraging its distinctive mechanisms of fast non-dominated sorting and crowding distance calculation, the NSGA-II algorithm efficiently handles these three competing objectives, searching for the Pareto optimal set within the complex solution space. Consequently, it provides the network with a range of feasible configuration strategies, spanning from 'communication-priority' to 'sensing-priority' options, with varying resource consumption levels.

Algorithm 1: NSGA-II for Multi-Objective Resource Optimization in OCC-ZC PRACH System

Require: Individual encoding: $\mathbf{w} \in \mathcal{W}_{\text{orthogonal}}$, $P \in [P_{\min}, P_{\max}]$, $B \in [B_{\min}, B_{\max}]$
Ensure: Pareto-optimal solution set P^*

procedure NSGA-II($N, G_{\max}, p_c, p_m$)
  Initialize P_0 with N feasible $(\mathbf{w}, P, B)$ configurations
  Evaluate each individual in P_0 on three objectives:
    1. $\eta_{\text{comm}}(\mathbf{w}, P, B)$: access success probability
    2. $\hat{\epsilon}_{\text{sensing}}(\mathbf{w}, P, B)$: normalized sensing error
    3. $\hat{C}_{\text{resource}}(P, B)$: resource consumption cost
  Non-dominated sort P_0, compute crowding distance
  $t \leftarrow 0$
  while $t < G_{\max}$ **do**
    $Q_t \leftarrow \emptyset$
    for $i = 1$ to $N/2$ **do**
      Select parents p_1, p_2 from P_t via binary tournament
      Crossover: hybrid operators with probability p_c:
        - For P, B: Simulated Binary Crossover (SBX)
        - For $\mathbf{w}$: Single-point crossover
      Generate offspring c_1, c_2
      Mutation: hybrid operators with probability p_m:
        - For P, B: Polynomial mutation
        - For $\mathbf{w}$: Random replacement in $\mathcal{W}_{\text{orthogonal}}$
      $Q_t \leftarrow Q_t \cup \{c_1, c_2\}$
    end for
    Evaluate all individuals in Q_t on the three objectives
    $R_t \leftarrow P_t \cup Q_t$
    Fast non-dominated sort $R_t \rightarrow \mathcal{F}_1, \mathcal{F}_2, \ldots, \mathcal{F}_k$
    $P_{t+1} \leftarrow \emptyset$
    $i \leftarrow 1$

 doi:10.20944/preprints202603.0126.v1

while $|P_{t+1}| + |\mathcal{F}_i| \leq N$ **do**
  Compute crowding distance for each in $\mathcal{F}_i$
  $P_{t+1} \leftarrow P_{t+1} \cup \mathcal{F}_i$
  $i \leftarrow i + 1$
end while
Sort $\mathcal{F}_i$ by descending crowding distance
$P_{t+1} \leftarrow P_{t+1} \cup$ first $(N - |P_{t+1}|)$ of $\mathcal{F}_i$
$t \leftarrow t + 1$
end while
$P^* \leftarrow$ non-dominated solutions from P_t (i.e., $\mathcal{F}_1$)
return P^*
end procedure

5. Performance Evaluation

5.1. Simulation Parameters

In this subsection, we evaluate the performance of the proposed OCC-ZC preamble in a low-altitude long-distance ISAC scenario.

The simulation parameters are summarized in Tables 1 and 2. We compare the proposed scheme with the conventional ZC-based PRACH scheme. The performance metrics include: (i) detection probability η_{comm} for communication; (ii) root mean square error (RMSE) of range and velocity estimation for sensing; (iii) Cramér-Rao lower bound (CRLB) for range and velocity as theoretical benchmarks. The impact of the weighting factor λ is also analyzed.

Table 1. Parameters for Communication Performance Simulation.

Parameter	Symbol	Value
Carrier Frequency	f_c	3.5 GHz
Transmit Power	P_{tx}	23 dBm
Channel Model	–	3GPP UMa LOS, Shadowing Std. $\sigma = 4$ dB
Reference Communication Range	R_0	2 km
ZC Sequence Length	N_{ZC}	839
Conventional Preamble Space	N_{trad}	64
Preamble Repetitions (OCC Length)	M	4
Access Evaluation Window	T_{win}	100 ms

Table 2. Parameters for Sensing Performance Simulation.

Parameter	Symbol	Value
Carrier Frequency	f_c	3.5 GHz
Transmit Power	P_{tx}	23 dBm
Channel Model	–	3GPP UMa LOS, Shadowing Std. $\sigma = 4$ dB
Reference Target Range	R_0	10 km 20 km 30 km 50 km
Reference Target Radial Velocity	v_0	60 m/s 70 m/s 80 m/s 100 m/s
Preamble Repetition Number	M	4

The selection of simulation parameters in Table 1 is designed to construct a rigorous and realistic evaluation scenario for long-distance communication access at low-altitude [27]. The carrier frequency is set to 3.5 GHz with a system bandwidth of 20 MHz, directly corresponding to the configuration of a mainstream 5G mid-band (e.g., n78 band). A transmit power of 23 dBm is selected to model the typical uplink transmission power level of current commercial aircraft communication payloads. The channel model adopts the 3GPP Urban Macrocell (UMa) line-of-sight model supplemented by log-normal shadowing with a standard deviation of 4 dB. This model effectively captures the

 doi:10.20944/preprints202603.0126.v1

channel characteristics in open airspace, such as suburban or campus areas, where a stable LOS path exists between the UE and the base station while subject to minor blockages from sporadic obstacles, providing propagation conditions with both stability and randomness.

A Zadoff-Chu sequence of length 839 is employed as the base preamble, and a conventional preamble space of 64 based on cyclic shifts is assumed per cell. This fully adheres to the standard design of long preambles in 4G/5G PRACH, ensuring a fair baseline for comparison between the proposed and conventional schemes. The core of the simulation is to observe the effect of the introduced "repetition" and "orthogonal covering" mechanism. Therefore, the repetition number M is set to 4 for comparison. All access attempts are evaluated within a fixed time window of 100 ms. This duration is adequate to encompass a complete four-step random access procedure and simulate certain retransmission processes.

The parameters in Table 2 are selected to evaluate sensing performance under realistic conditions [28]. The carrier frequency $f_c = 3.5$ GHz and signal bandwidth $B = 20$ MHz together form a typical sub-6GHz carrier configuration of 5G NR . The transmit power $P_{tx} = 23$ dBm mimics the typical uplink transmission power level of commercial aircraft communication payloads. The channel model adopts the 3GPP UMa line-of-sight model supplemented with moderate shadow fading ($\sigma = 4$ dB), characterizing the channel features where a dominant line-of-sight path exists between the UE and the base station in suburban or campus environments, yet is subject to minor blockages from sporadic obstacles.

5.2. Communication Performance

This subsection evaluates the communication performance of the proposed OCC-ZC preamble in terms of detection probability.

Figure 5 compares the detection probability of the conventional ZC preamble and the proposed OCC-ZC preamble under varying SNR. The OCC-ZC scheme achieves a detection probability of 1 at an SNR of 10 dB, while the conventional scheme requires 15 dB. Furthermore, throughout the entire SNR range, the OCC-ZC PRACH curve consistently lies above the conventional PRACH curve, demonstrating its performance advantage under various channel conditions. This improvement stems from the additional orthogonal dimension introduced by OCC, which enhances the distinguishability of preambles.

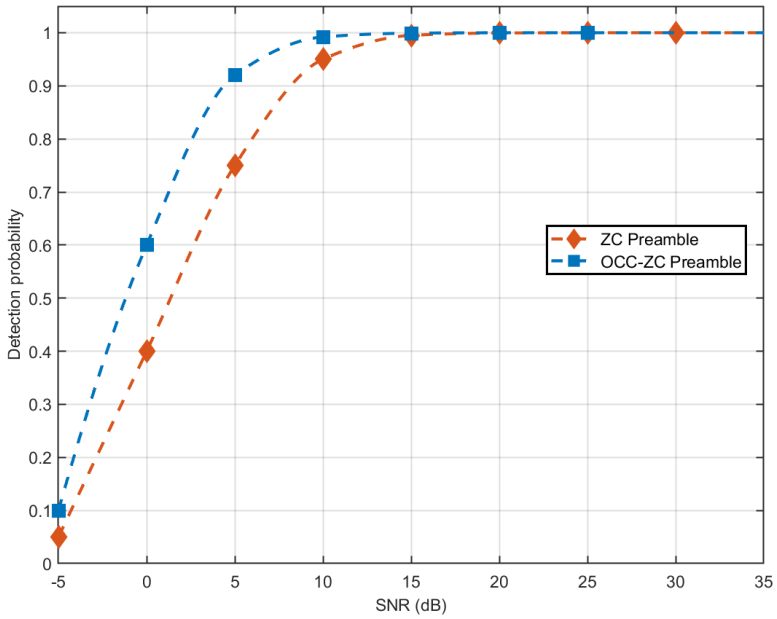

Figure 5. Performance Comparison of Detection Probability.

The detection probability performance of the OCC-ZC preamble under different system strategies is further investigated and the evaluation results are shown in Figure 6.

 doi:10.20944/preprints202603.0126.v1

The detection probability performance of three representative configurations selected from the obtained Pareto-optimal solution set, which corresponds to the sensing-priority, balanced, and communication-priority strategies, is compared. As shown in Figure 6, these three configurations, originating from different trade-off points on the Pareto front, exhibit significant differences in detection performance. In the low-SNR region (SNR $<$ 15 dB), the communication-priority configuration demonstrates a clear detection advantage, achieving a near-unity detection probability at SNR $\approx$ 15 dB. In contrast, the sensing-priority configuration yields a lower detection probability at the same SNR levels, requiring SNR $\approx$ 25 dB to reach comparable performance. The performance of the balanced configuration lies between these two extremes. This result visually illustrates the characteristics of different solutions along the Pareto frontier and validates the inherent resource trade-off between communication and sensing functions: higher requirements for sensing accuracy typically come at the cost of reduced access reliability.

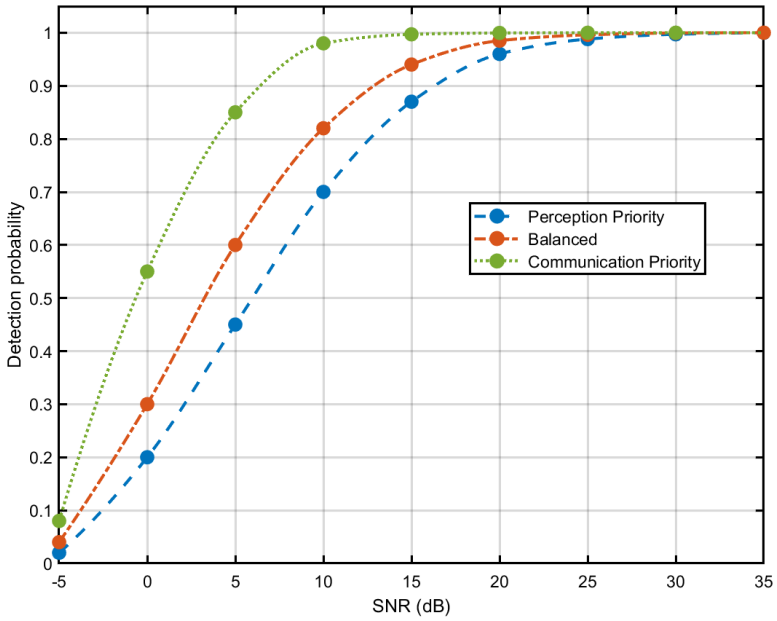

Figure 6. Detection Probability under Different Communication-Sensing Trade-offs.

5.3. Sengsing Performance

The sensing performance of the proposed PRACH preamble scheme in terms of range and velocity estimation accuracy is evaluated as follows.

As shown in Figure 7, the distance estimation performance based on the OCC-ZC preamble is evaluated. The graph illustrates the relationship between the root mean square error (RMSE) of distance estimation and the signal-to-noise ratio (SNR) for four different target distances (10km, 20km, 30km, and 50km). It can be observed that all curves exhibit a typical trend of rapid decline followed by a slower decrease. In the low SNR region (-10 dB to 0 dB), the distance estimation error decreases quickly as the SNR increases, primarily because noise is the dominant factor in this range, and improving the SNR significantly enhances signal quality. In the high SNR region (10 dB to 20 dB), the rate of error reduction slows down, indicating that the system is gradually approaching its theoretical performance limit. In addition, the target distance has a significant impact on the accuracy of the estimation. Under the same SNR condition, the estimation error increases with a greater distance. This difference primarily stems from two factors: first, signal attenuation increases with the square of the distance, leading to a decrease in received signal power; second, multipath effects become more pronounced under long-distance conditions. Notably, even at a long distance of 50km, when the SNR reaches 20 dB, the system can still achieve a positioning accuracy of about 10m, which fully demonstrates the effectiveness of the proposed OCC-ZC preamble in low-altitude long-distance ISAC scenarios.

 doi:10.20944/preprints202603.0126.v1

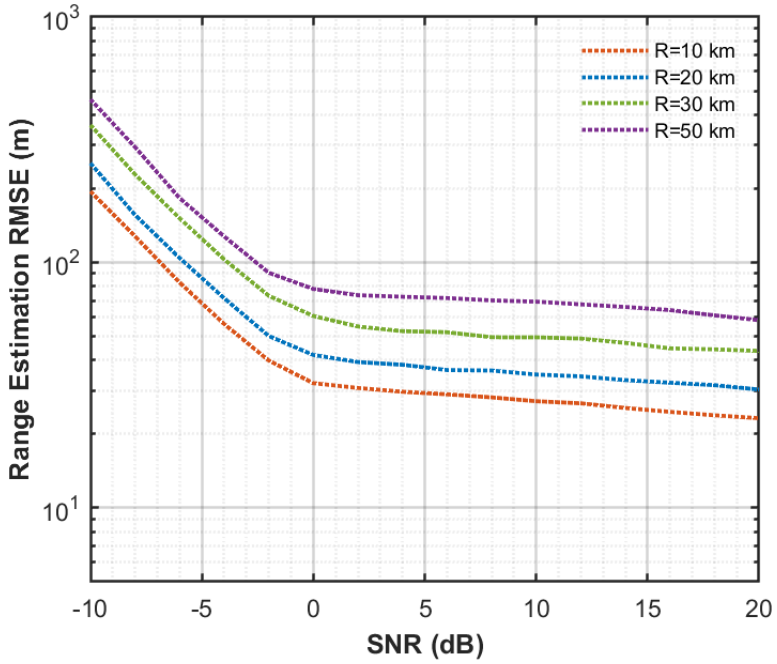

Figure 7. Range Estimation Performance.

The Figure 8 illustrates the velocity estimation performance, examining the variation of velocity estimation RMSE with SNR for four different target velocities (60 m/s, 70 m/s, 80 m/s, and 100 m/s). Similar to distance estimation, the velocity estimation error also shows a decreasing trend as SNR increases, exhibiting the same characteristic of rapid decline followed by a slight decrease.

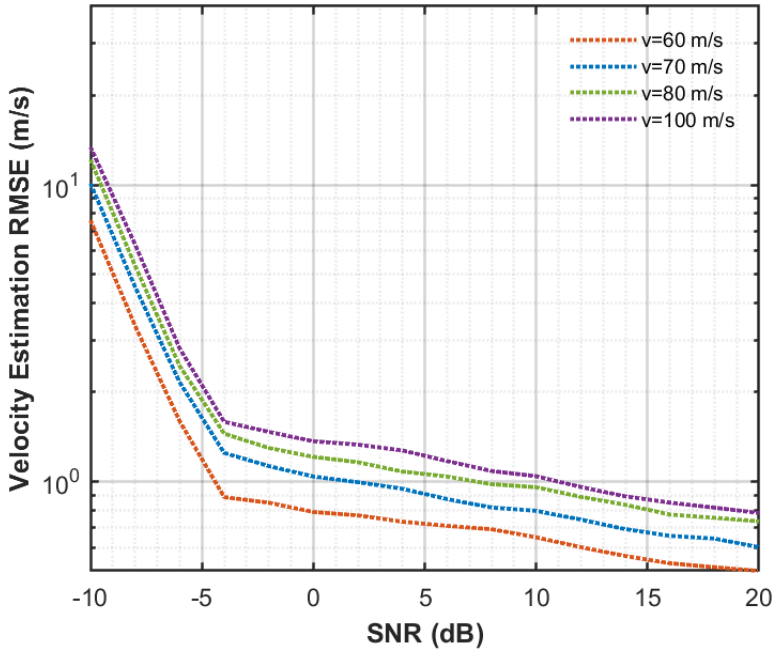

Figure 8. Velocity Estimation Performance.

Under identical SNR conditions, targets with lower speeds (e.g., 60m/s) typically exhibit lower estimation errors, whereas targets with higher speeds (e.g., 100m/s) show relatively larger errors. This discrepancy primarily stems from the estimation mechanism of Doppler shift: the Doppler shift for low-speed targets is smaller, while for high-speed targets, the larger Doppler shift is easier to detect but also more susceptible to issues like phase ambiguity. Notably, even under high-speed conditions of 100m/s, the system can still achieve a velocity estimation accuracy of approximately 0.2 m/s when

 doi:10.20944/preprints202603.0126.v1

the SNR reaches 15 dB. This is of significant importance for the precise sensing of low-altitude mobile platforms such as aircraft.

Figures 9 and 10 compare the Cramér-Rao lower bound (CRLB) for range and velocity estimation [29], respectively. The proposed OCC-ZC scheme outperforms the conventional ZC scheme and approaches the ideal sensing bound, confirming its theoretical superiority in sensing accuracy.

By comparing Figure 7 with Figure 9 and Figure 8 with Figure 10, it can be observed that the RMSE curves of the range and velocity estimates obtained using the OCC-ZC preamble approach the corresponding $\sqrt{\text{CRLB}}$ values as the SNR increases. This indicates that the proposed estimator is asymptotically efficient. The alignment between simulation and theory (35) confirms that the OCC-ZC preamble enables near-optimal estimation accuracy in both range and velocity under high SNR conditions.

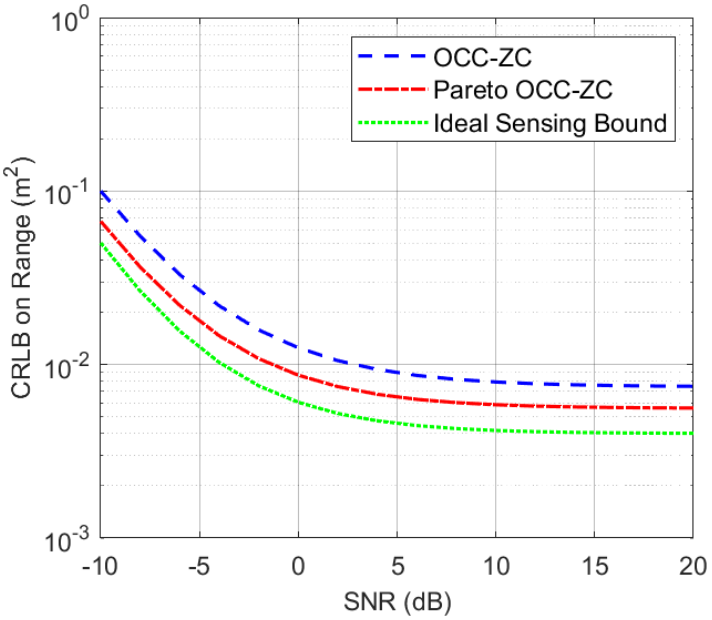

Figure 9. Comparison of performance in terms of the CRLB on range.

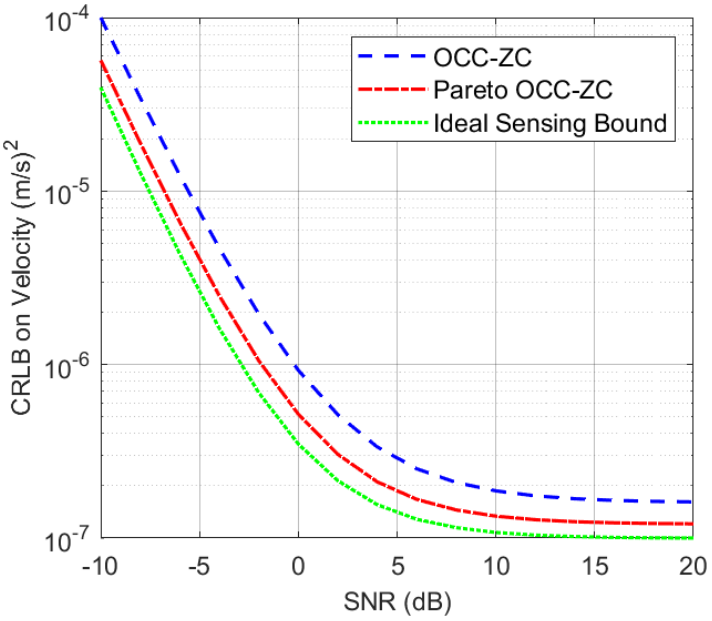

Figure 10. Comparison of performance in terms of the CRLB on velocity.

 doi:10.20944/preprints202603.0126.v1

5.4. Multi-Objective Optimization

To comprehensively analyze the trade-off among communication performance, sensing accuracy, and resource efficiency, we first present the Pareto frontier obtained by the NSGA-II algorithm in Figure 11. The three axes represent detection probability η_{comm}, sensing error $\epsilon_{\text{sensing}}$, and resource cost $\hat{C}_{\text{resource}}$. The Pareto front clearly illustrates the inherent trade-offs among these three objectives [23].

Furthermore, the color gradient from red to blue intuitively maps the differences in resource cost levels, clearly demonstrating the decisive impact of resource investment on system performance: solutions with low resource cost cluster in regions characterized by lower detection probability and higher sensing errors, whereas those with high resource cost achieve both high detection probability and low sensing errors.

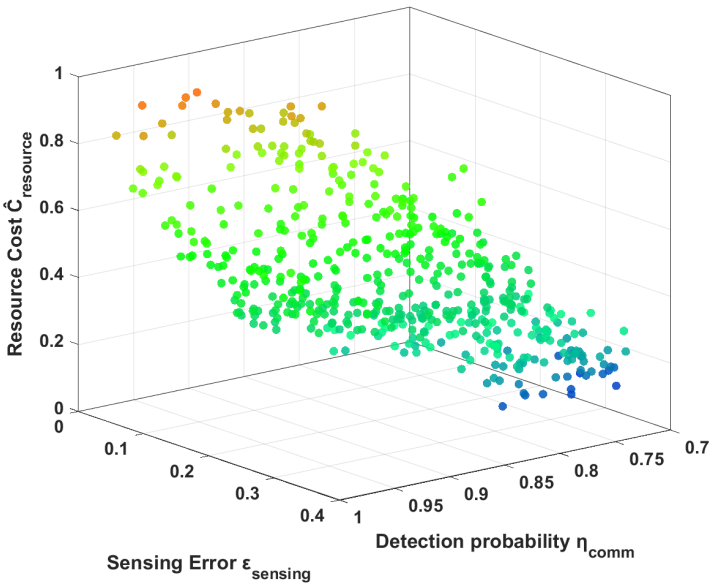

Figure 11. Pareto Frontier in three-dimensional objective space.

Figures 12 and 13 further depict the relationships between resource cost and detection probability, and between resource cost and sensing error, respectively. As resource investment increases, both communication reliability and sensing accuracy improve, but the marginal gain diminishes beyond a certain point, indicating the need for balanced resource allocation.

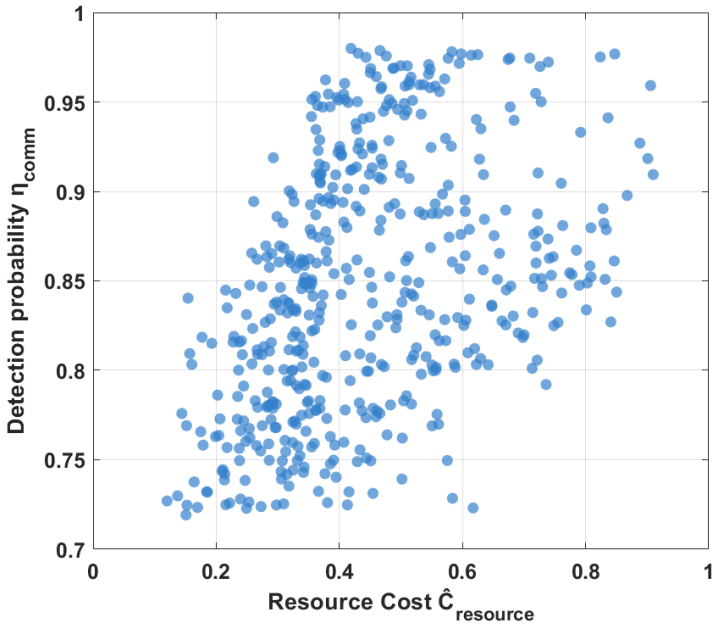

Figure 12. Resource Cost $\hat{C}$resource vs Detection probability ηcomm.

 doi:10.20944/preprints202603.0126.v1

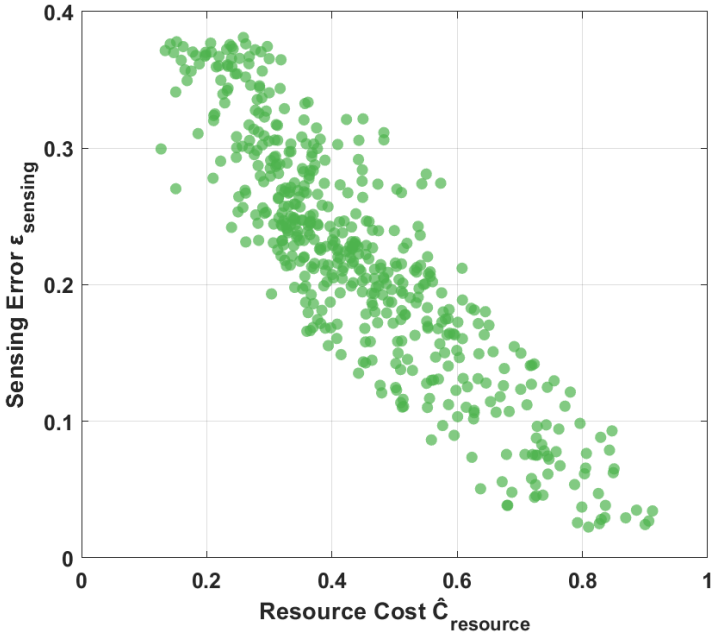

Figure 13. Resource Cost $\hat{C}$resource vs Sensing Error ϵsensing.

Figure 14 illustrates the relationship between the detection probability η_{comm} and the sensing error $\tilde{\epsilon}_{\text{sensing}}$. The scatter plot reveals that as the detection probability increases, the sensing error exhibits a decreasing trend, demonstrating a co-improvement relationship between the two metrics. This phenomenon fundamentally stems from our proposed OCC-ZC structure design, where the repetition count M serves as the core parameter for simultaneously optimizing both performance indicators. An increase in M expands the orthogonal preamble space, significantly reducing the collision probability during the random access process, thereby enhancing the detection probability. On the other hand, it provides more time-domain observation samples for the sensing function, substantially improving the accuracy of Doppler frequency shift and range estimation through coherent combining gain, which in turn reduces the sensing error.

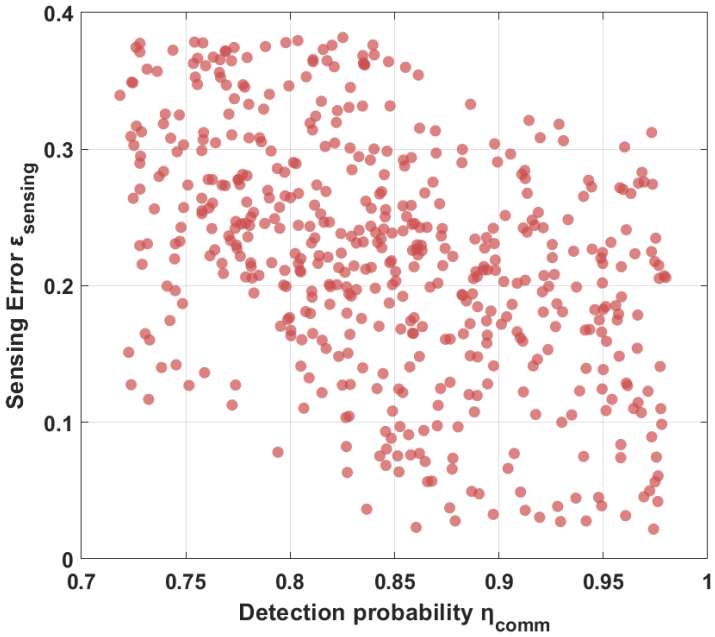

Figure 14. Detection probability η_{comm} vs Sensing Error $\tilde{\epsilon}_{\text{sensing}}$.

The simulation results demonstrate that the proposed OCC-ZC preamble scheme successfully integrates sensing capabilities into the PRACH access procedure. Compared with conventional access

 doi:10.20944/preprints202603.0126.v1

schemes, it achieves superior detection probability for random access while simultaneously providing accurate estimation of range and velocity. The closed-loop optimization framework governed by the weighting factor λ enables flexible trade-offs between communication reliability and sensing accuracy. This verifies that the proposed scheme is an efficient solution for low-altitude long-distance ISAC systems, achieving the design goal of "sensing before access completion".

6. Conclusions

In this paper, we propose an enhanced PRACH preamble scheme suitable for low-altitude long-distance integrated sensing and communication systems, aiming to deeply embed sensing capabilities into the PRACH, enabling the network to possess target sensing abilities from the very beginning of access. We derive the CRLB for distance and velocity estimation when using the OCC-ZC preamble scheme, establish detection probabilities in communication, and then formulate a multi-objective optimization problem. To solve this non-convex problem, we propose using the NSGA-II algorithm to optimize multiple variables. Simulation results across various test scenarios numerically demonstrate the feasibility and reliability of the proposed method.

Author Contributions: Conceptualization, W.XY., Y.XY., and Y.X.; methodology, Y.XY, X.ZC., Z.ZH., and M.Q.; software, Z.ZH., M.Q., and S.ZJ.; validation, W.XY. and Y.XY.; formal analysis, Z.ZH., Y.XY. and Y.X.; investigation, W.XY., Y.XY., Y.X., X. ZC, and Z.ZH.; resources, Z.ZH., M.Q., and S.ZJ.; data curation, Z.ZH., M.Q., and S.ZJ.; writing-original draft preparation, W.XY., Y.XY., Z.ZH., and M.Q.; writing-review & editing, Y.XY., Y.X. and X.ZC; visualization, M.Q., Z.ZH., and S.ZJ.; supervision, Y.XY.; project administration, W.XY., Y.X., X.ZC., and Y.XY.; funding acquisition, W.XY, X.ZC. All authors have read and agreed to the published version of the manuscript.

Funding: This research was funded by CRSC Low-Altitude Intelligence Technology Co., Ltd. of funder grant number 6800-K1240008.

Conflicts of Interest: The authors declare no conflicts of interest. The funders had no role in the design of the study; in the collection, analyses, or interpretation of data; in the writing of the manuscript; or in the decision to publish the results.

References

1. Jing, X.; Liu, F.; Masouros, C. et al. ISAC from the sky: UAV trajectory design for joint communication and target localization. *IEEE Transactions on Wireless Communications* **2024**, *23*(10), 12857–12872.
2. Du, Z.; Liu, F.; Li, Y.; Yuan, W.; Cui, Y.; Zhang, Z.; Masouros, C.; Ai, B. Toward ISAC-Empowered Vehicular Networks: Framework, Advances, and Opportunities. *IEEE Wireless Communications* **2026**, *32*(2), 222–229.
3. Shang, C.; Yu, J.; Hoang, D. T. Energy-Efficient and Intelligent ISAC in V2X Networks with Spiking Neural Networks-Driven DRL. *IEEE Transactions on Wireless Communications* **2026**, *25*(2), 1–15.
4. Hua, M.; Wang M.; Yang W.; You X.; Shu F.; Wang J.; Sheng W. and Chen Q. Analysis of the frequency offset effect on random access signals. *IEEE Transactions on communications* **2013**, *61*(11), 4728–4740.
5. Hua, M.; Wang, M.; Yang, K. W.; Zou, K. J. Analysis of the Frequency Offset Effect on Zadoff–Chu Sequence Timing Performance. *IEEE Transactions on Communications* **2014**, *62*, 4024–4039.
6. Liu, Y.; Niyato, D.; Shim, B.; et al. Cell-Free Integrated Sensing and Communication: Principles, Advances, and Future Directions. *arXiv* **2025**, *submitted*.
7. 3GPP TSG-RAN1. TR 38.901-Rel-20: Study on channel model for ISAC. *3GPP Technical Report* **2025**, *in press*.
8. Yin H.; Huang Y.; Han L.; et al. Thoughts on 6G integrated communication, sensing and computing networks. *Scientia Sinica Informationis* **2023**, *53*, 1838–1842.
9. Liu F.; Yuan W.; Masouros C.; et al. Toward dual-functional radar-communication systems: Optimal waveform design. *IEEE Transactions on Signal Processing* **2018**, *66*, 4264–4279.
10. 3GPP TSG-RAN WG1. TS 38.321 v17.4.0: Medium Access Control (MAC) protocol specification; §5.1 Random Access Procedure. *3GPP Technical Specification* **2023**, *in press*.
11. 3GPP TSG-RAN WG1. TS 38.211 v17.5.0: Physical channels and modulation; §6.3.3 PRACH preamble generation. *3GPP Technical Specification* **2023**, *in press*.
12. Chen, H.; Wang, P.; Li, S.; Lin, S.; Wang, Z.; Fang, C. A Novel Preamble Design for 5G Enabled LEO Non-Terrestrial Networks. In Proceedings of the 2022 IEEE Global Communications Conference (GLOBECOM 2022), Rio de Janeiro, Brazil, 4–8 December 2022; pp. 680–686.

 doi:10.20944/preprints202603.0126.v1

13. Yang, H. Q.; Dai, J. Y.; Li, H. D.; et al. Adaptively programmable metasurface for intelligent wireless communications in complex environments. *Nat. Communications* **2026**, *16*, 6070.
14. Wu, Y.; Lian, Z.; Dang, S.; Shihada, B. *Digital Twin-Empowered Computing in Integrated Sensing, Communication, and Computing Networks: A Survey.* IEEE Internet of Things Journal 2024, *11* , 21153-21177.
15. Wang, Z.; Wang, L.; Zhu, D.; Liu, Q.; Li, T. *Detection of Low-Slow-Small Targets in Complex Environments Based on an Efficient Scattering Network.* Remote Sensing 2024, *16* , 388.
16. Wang, Y.; Su, Z.; Gao, Y.; Ba, J. *Key Technologies for Low-Altitude Internet Networks: Architecture, Security, and Optimization.* Journal of Electronics & Information Technology 2025.
17. Wang, B.; Luo, P.; Yang, Y.; Zhao, Z.; Dong, R.; Guan, Y. *A Review and Prospect of Cybersecurity Research on Air Traffic Management Systems.* Journal of Electronics & Information Technology 2025, *47* , 1230–1265.
18. Khan, H. A.; Khan, H.; Ghafoor, S.; et al. *A Survey on Security of Automatic Dependent Surveillance-Broadcast (ADS-B) Protocol: Challenges, Potential Solutions and Future Directions.* IEEE Communications Surveys & Tutorials 2024.
19. Jiang, X.; Li, H.; Zhang, W. *Optimization of PRACH Configuration Parameters in LTE Networks: A Review and Future Directions.* IEEE Communications Surveys & Tutorials 2025, *27*, 456–478.
20. Linsalata, F.; Albanese, A.; Sciancalepore, V.; Roveda, F.; Magarini, M.; Costa-Perez, X. OTFS-superimposed PRACH-aided Localization for UAV Safety Applications. In Proceedings of the 2021 IEEE Global Communications Conference (GLOBECOM), Madrid, Spain, 7–11 December 2021; pp. 1–6.
21. Kumari, P.; Vorobyov, S. A.; Heath, R. W. Adaptive Virtual Waveform Design for Millimeter-Wave Joint Communication–Radar. *IEEE Transactions on Signal Process.* **2020**, *68*, 715–730.
22. Deb K; Pratap A; Agarwal S; et al. A fast and elitist multiobjective genetic algorithm: NSGA-II. *IEEE Transactions on Evolutionary Computation* **2002**, *6*, 182–197.
23. Ma, Y.; Wang, X.; Guo, Y.; Li, B. Many-objective evolutionary algorithm based on curvature estimation of Pareto front. *Journal of Software* **2023**, *34*(6), 1890–1907.
24. Gregoratti D; Arteaga X; Broquetas J. Mathematical Properties of the Zadoff-Chu Sequences. *arXiv preprint* **2023**, arXiv:2311.01035.
25. Schaich, F. Orthogonal Modulation and Code Division Multiplexing Techniques. In *Multi-Carrier Spread-Spectrum*; Fazel, K., Kaiser, S., Eds.; Springer: Dordrecht, The Netherlands, 2006; pp. 47–56.
26. Tao, J.; Yang, L. Improved Zadoff-Chu Sequence Detection in the Presence of Unknown Multipath and Carrier Frequency Offset. *Journal/Conference Name* **2018**, *Vol.*, Pages.
27. Guidotti, A.; Vanelli-Coralli, A.; Andrenacci, S.; Colavolpe, G.; Kodrinos, A.; Luglio, M. Random Access Procedure in Non-Terrestrial 5G Networks. *IEEE Access* **2021**, *9*, 117535–117548.
28. Zhang, H.; You, C.; Wang, X.; Song, L.; Zheng, L. Integrated Location Sensing and Communication for Ultra-Massive MIMO With Hybrid-Field Beam-Squint Effect. In Proceedings of the IEEE Global Communications Conference (GLOBECOM 2024), Kuala Lumpur, Malaysia, 6–10 December 2024; pp. 1–6.
29. Kay S M. *Fundamentals of Statistical Signal Processing, Volume I: Estimation Theory*; Prentice Hall: Upper Saddle River, NJ, USA, **1993**.